Received: 22 December 2024 | Revised: 15 February 2025 | Accepted: 17 February 2025

DOI: 10.1002/pc.29732

RESEARCH ARTICLE

Polymer COMPOSITES WILEY

Experimental and numerical investigation of susceptor-aided continuous induction welding of low-melt PAEK composites

Francesca Lionetto[1] | **Giulio Zecca**[1] | **Giuseppe Buccoliero**[2] | **Sonia Bagheri**[1] | **Claudio Mele**[1]

[1]Department of Engineering for Innovation, University of Salento, Lecce, Italy

[2]Advanced Materials and Processes Consulting Department, CETMA, Brindisi, Italy

Correspondence
Francesca Lionetto, Department of Engineering for Innovation, University of Salento, via per Monteroni, 73100 Lecce, Italy.
Email: francesca.lionetto@unisalento.it

Abstract

This study enhances the continuous induction welding of unidirectional carbon fiber-reinforced low-melt PAEK, addressing the challenge posed by the anisotropic electrical conductivity of carbon fibers, which causes uneven eddy current distribution, inadequate heating, and weak joint strength. A metallic susceptor moving with the coil along the weld line but not remaining in the bonding interface was introduced to selectively heat the weld area, preventing unnecessary matrix melting. Experimental validation and Finite Element (FE) simulations confirmed the approach's effectiveness in achieving uniform heating and stronger joints. A key parameter in 3D simulation was the electrical conductivity of the laminate, which was lay-up dependent and challenging to measure directly. This work proposed a novel method to estimate electrical conductivity for anisotropic materials by aligning measured and simulated temperature profiles during static induction welding. The model accurately predicted temperature distribution and crystallinity at the interface under different coil speeds. Results demonstrated the feasibility of using a removable steel susceptor to enhance continuous induction welding of UD carbon fiber laminates with a low-melt PAEK matrix. The proposed experimental and numerical approach offers a valuable tool for defining a processing window and optimizing stacking sequences, improving the induction welding of UD carbon fiber composites and non-conductive fiber laminates.

Highlights

- Continuous induction welding of unidirectional carbon fiber-reinforced composites.
- Induction heating assisted by a movable steel susceptor.
- Composite electric conductivity determined by an iterative numerical procedure.
- Temperature prediction during continuous induction welding.
- Crystallinity prediction as a function of coil speed during induction welding.

KEYWORDS

finite element analysis, heat generation, induction welding, numerical simulation, thermoplastic composites

1 | INTRODUCTION

Carbon fiber-reinforced polymers (CFRPs) are widely employed in structural applications in the aerospace and automotive industries due to their remarkable mechanical and chemical properties.[1,2] They are well-suited for applications requiring a high strength-to-weight ratio, vibration damping, corrosion resistance, and customizable properties to meet specific requirements.[3,4] Very recently, the efforts toward sustainability in the composite industry have highlighted the need for innovative approaches both in the material choice and in the design and assembly of composite components.[5–7] In this context, the recyclability of thermoplastic matrices, in addition to high chemical and corrosion resistance, good impact properties, high damage tolerance, unlimited shelf life, low storage costs, and weldability, has sparked a growing interest in thermoplastic matrix composites as a valid alternative to thermosetting matrix composites for sustainable composite manufacturing.[8–10] On the other hand, there is also an ongoing concern about the contribution of thermoplastic composites to the microplastics problem when they degrade or break down over time, particularly in marine environments.[11,12] CFRP joining methods can be categorized into "hot joining" and "cold joining." Hot joining involves applying heat and pressure to the joint interface to achieve bonding. In contrast, cold joining methods rely on techniques, such as adhesive bonding and mechanical fastening.[13] Regarding the welding of thermoplastic composites, fusion bonding techniques offer solutions to the drawbacks of mechanical fastening, which leads to stress concentrations from drilled holes and increased weight, as well as the challenges of adhesive bonding including extensive surface preparation and long curing times.[14,15] Welding is essential in composite manufacturing, enabling the efficient joining of different materials while ensuring structural integrity and enhancing the overall performance of composite components in various industrial applications.[16,17] The most common welding methods for thermoplastic matrix composites include resistance,[18,19] ultrasonic welding,[20–22] and induction welding.[23–26]

Induction welding, initially developed in the 90s, has regained interest due to its ability to deliver strong mechanical properties, such as high compression and shear resistance to stiffened panels, while offering several processing advantages, such as short welding times, high efficiency, high repeatability, low energy consumption, non-contact processing, ease of automation, and the possibility of continuous welding.[27,28] Recently, induction welding has also been proposed for repairing damaged thermoplastic composite laminates.[29,30] This electromagnetic welding technique is based on a high-frequency oscillating electric current flowing through an inductor or coil, generating an alternating magnetic field in the surrounding area. This magnetic field induces eddy currents, resulting in induction heating within electrically conductive materials located near the coil.[31] In carbon fiber-reinforced polymers, induction heating occurs thanks to the electrically conductive carbon fibers through three mechanisms: (a) Joule heating from eddy currents circulating in closed loops formed by the fibers, (b) heating due to contact resistance between fibers at their junctions, and (c) dielectric hysteresis heating of the polymer at the fiber-matrix interface, where the fibers act as capacitors separated by a dielectric layer of thermoplastic resin.[32,33] The induced heating softens and melts the matrix softening and melting, enabling further processing and joining under pressure. For over three decades, researchers have studied the welding of thermoplastic composites using conductive patterns in carbon fiber-reinforced fabric stacks. Eddy currents are relatively easily generated in woven fabric composites, where the interlacement of bundles allows for contact between perpendicular fibers, creating a conductive loop. In contrast, in unidirectional (UD) plies, the highly anisotropic nature with a very low transverse electrical conductivity limits the formation of eddy currents in a ply. Instead, the ability to generate eddy currents in UD laminates depends on the through-thickness conductivity of the plies and the contact resistance at the interfaces between plies with different fiber orientations.[34]

Recently, the joining of unidirectional (UD) laminates has gained significant attention from researchers since UD prepregs and tapes are finding wide use in the composite industry due to improved fiber orientation control and the cost-efficiency they offer. These materials contribute to high-performance composites for structural applications providing enhanced strength, stiffness, toughness, and fatigue resistance.[35] The limited induction heating capabilities of UD laminates, caused by the absence of fiber-crossing, can be addressed by using a susceptor, a conductive material placed at the interface between the two adherents. The susceptor absorbs electromagnetic energy and converts it into heat, which is then transferred to the adherents mostly through conduction.[36,37] The presence of a susceptor can lead to challenges, such as uneven

temperature distribution during welding of UD laminates, which may result in drawbacks like diminished adhesive strength, stress concentrations within the composite, mismatches in thermal and electrical conductivity, increased susceptibility to corrosion, and added weight.[36,38,39] Temperature inconsistencies can promote porosity, a major defect that reduces material properties and, in some cases, necessitates the rejection of part.[40] Overheating, indeed, may cause thermal degradation of the matrix, forming voids in the weld joint. Excessive heat can also cause thermal degradation of the matrix, resulting in void formation within the weld joint. At the same time, insufficient heating can prevent the complete melting of the thermoplastic matrix, hindering proper material flow and allowing air or gases to become trapped within the joint. Achieving an optimal heating profile and carefully balancing the process parameters are thus essential to minimize porosity and produce reliable, high-quality welds in thermoplastic composites.

In industrial applications, continuous induction welding, where the coil moves along the joint, is gaining growing interest due to its potential for fast automation. However, the control of the temperature distribution during continuous induction welding is a very challenging task. Heat transfer depends both on the process parameters (frequency, input power, applied pressure, coil speed and welding time) and the material properties, such as fiber architecture and lay-up, polymer matrix, and so forth.[41] The interaction between electromagnetic and thermal phenomena makes heat transfer during induction welding a highly complex multi-physics process.

While already utilized in the composite industry, induction welding still depends on costly and time-consuming trial-and-error methods to establish optimal processing parameters. Numerical simulation is a powerful tool for predicting temperature evolution during continuous induction welding, which is critical for optimizing the process and avoiding damage from surface overheating. Predictive simulations also help to reduce the time and costs required for process development.[34] A key parameter in simulating induction welding is the electrical conductivity of the composite material, a highly anisotropic property with very high values along the fiber direction and extremely low values in the transverse direction.[42] Moreover, most current simulations of continuous induction welding have focused on woven fabric-reinforced laminates,[33] with few studies addressing UD laminates.[34,43] Recently, De Wit et al.[44] measured the electrical conductivities of both UD plies and cross-plies laminates and simulated the induction heating during static welding. Moreover, Polydoropoulou et al.[45] calculated the electrical conductivities of UD laminates by a homogenization approach to be used in numerical models for simulating continuous induction welding. However, determining the electrical conductivity of UD carbon fiber-reinforced polymers, whether through direct measurement or homogenization methods, presents significant challenges and limitations due to its anisotropic nature and strong dependence on the composite lay-up.[42,46]

This work aimed to set up a reliable technological approach for the continuous induction welding of UD laminates and the determination of the electrical conductivity of UD laminates with different stacking sequences. The novelty of this route was based on induction heating assisted by a mobile steel susceptor, attached to the welding head, which was moved at the same speed as the induction coil along the weld line but did not remain at the welding interface after welding unidirectional carbon fiber laminates with a low-melt Poly Aryl Ether Ketone (LMPAEK) composite.[47,48] In this way, a reduction in the welded joint properties was prevented. A compaction roller applied pressure between the adherents while cooling them. LMPAEK belongs to the Poly(aryletherketones), a polymer family with outstanding mechanical properties, thermal stability, and chemical resistance, making them increasingly attractive as thermoplastic matrices for high-performance composite applications, in particular in aerospace and automotive.[49–52] LMPAEK presents several advantages compared to the well-known PEEK, first of all, lower melting and processing temperatures, thus reducing energy consumption during processing, but with nearly identical mechanical properties and very close glass transition temperature Tg to PEEK.[53,54] Moreover, LMPAEK crystallizes more slowly than PEEK, leading to improved processability and enhanced bonding in welding, due to the extended molten state.[55] For these processing benefits, LMPAEK is gaining increasing attention because of LMPAEK. For these processing benefits, LMPAEK is gaining increasing attention in high-performance composite applications.[56,57] Although the induction welding of CF/PEEK composites has been widely studied, research on CF/LMPAEK induction welding is now emerging, with few reports available in the literature.[37]

Another novelty element of the present study consisted of the determination of the electric conductivity of the composite with an iterative procedure based on an FE model of static induction welding. The temperature distribution on the susceptor and at the interface between the two laminates, validated by temperature measurements, was correctly predicted and can be adjusted by modulating coil current intensity, distance from the top laminate, and speed of the coil. The weld quality was assessed through mechanical testing of single-lap-shear strength (SLSS) and optical microscopy of failure surfaces.

Figure 1 shows the workflow of the experimental and modeling activities presented in this work. The experimental work involved collecting input parameters for the

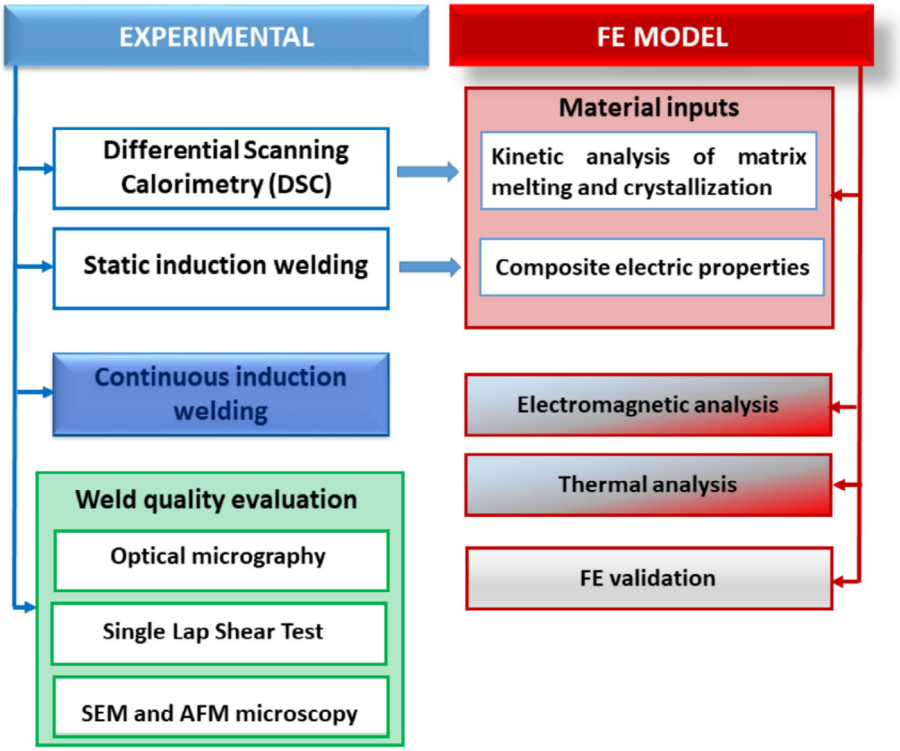

FIGURE 1 Scheme of the present research.

simulation, focusing on the thermal behavior of the LMPAEK matrix during melting and crystallization, which was both studied and modeled. Additionally, the electrical conductivity of the composite stack was determined, as will be explained later. Continuous induction welding was performed, and the quality of the resulting joint was assessed using micrography, single-lap shear testing, and surface fracture analysis. The finite element (FE) model combined electromagnetic field analysis with heat transfer in solids to simulate the process.

2 | EXPERIMENTAL

2.1 | Materials

The composite used in this study was manufactured from a unidirectional prepreg made of T700 carbon fibers (CF) with a fiber volume fraction of 58% and a low-melt Polyaryletherketone (LMPAEK) matrix. Composite laminates (250 mm × 150 mm × 3.7 mm) with $[GF/\pm 45/0/90/\mp 45/0/\pm 45/0]_s$ lay-up (Figure S1) were produced by compression molding in a hot press for 20 min at 340 °C and 2 MPa. A glass fiber/LMPAEK ply (48 g/m^2) was added to the surface of the thermoplastic UD laminate to prevent galvanic corrosion during component service life, as specified by the manufacturer.

The density and thermal properties of the composite laminates were determined starting from the individual properties of fibers and matrix, using the micromechanics equations.[58] In-plane electrical properties (σ_x, σ_y, σ_z) of the composite laminate were found through an iterative process using the data from a static induction heating test, achieving temperature convergence between the experimental data and FE analysis results, as explained later in the results section. Table 1 summarizes the properties considered for the CF/LMPAEK laminate.

2.2 | Characterization

The thermal properties of the LMPAEK matrix in Table 1 were determined by Differential Scanning Calorimetry (DSC). A Mettler Toledo DSC1 calorimeter was used to perform three subsequent dynamic scans on each sample: a heating from 25 to 360 °C, a cooling from 360 to 25 °C, and a second heating from 25 to 360 °C. The heating/cooling rate was 10 °C/min at a nitrogen flow of 50 mL/min. Three replicates were analyzed.

The surface temperature during induction welding was monitored by a FLIR A35 thermal imaging camera. The software Optis Pix Connect provided the temperature profiles.

The temperature at the welding interface was measured by K-type thermocouples with shielded cables connected to a Pico TC-08 data logger.

The mechanical properties of the welded joints were measured by single lap shear strength (SLSS) tests according

TABLE 1 Properties of the matrix, reinforcement and composite.

	ρ (kg/m^3)	C_p (J/kgK)	K (W/mK)	σ (S/m)	ε_r (–)	Reference
CF	1800	754	9.62	62,500	3.30	[59]
LMPAEK	1320	1410	0.22	10^{-15}	3.07	[60]
CF/LMPAEK laminate	1590	977	$k_x = k_y = 5.11$ $k_z = 0.62$	$\sigma_x, \sigma_y = 2070$ $\sigma_z = 0.15$	3.22	This work

to the ASTM D5868 standard using an MTS Insight 100 dynamometer with a crosshead speed of 2 mm/min and a 10 kN load cell. The apparent lap shear strength of six induction welded joints was calculated as the maximum load divided by the total overlap area (20 × 25 mm^2).

The morphological characterization of the cross-sections of induction welded joints was carried out using a Carl Zeiss Axio Imager A2M optical microscope. The samples were polished using 800 and 2400-grit-size silicon carbide grinding paper.

The specimens tested in single lap mode were cut with a diamond disc, and their fracture surfaces were analyzed by scanning electron microscopy (SEM) using a ZEISS EVO 40 microscope and by atomic force microscopy (AFM) using a MultiMode 8 AFM system in contact mode with a Silicon RTESPA cantilever.

2.3 | Induction welding equipment

The induction welding setup shown in Figure 2 was developed by Cetma and Sinergo (Italy) and was based on an ABB IRB 4600 robot with a six-axis articulated arm. Welding was performed with a 250 kHz, 220 V induction generator and a "double D" coil. The setup was equipped with a control system for the electric current flowing in the coil, which was based on the measurement of the surface temperature using an optical pyrometer. The distance between the coil and the upper adherent was equal to 2.6 mm. A cooled compaction roller with a diameter of 50 mm, placed at a distance of 36 mm far from the coil center, applied the consolidation pressure.

Continuous induction welding was realized using a 0.2 mm thick removable AISI 1095 steel susceptor placed at the welding interface, as shown in Figure 2. The susceptor was connected to the welding head, enabling it to move at the same speed as the coil, and be removed from the weld interface before applying the consolidation pressure. Due to the high electrical conductivity of steel, eddy currents were efficiently generated in the susceptor raising the temperature at the interface beyond the melting point of the composite matrix. An infrared lamp was positioned ahead of the coil to raise the surface temperature of the upper laminate.[14] The temperature at the surface of the top laminate was controlled by a pyrometer keeping a set point of 260 °C obtained after several experiments in continuous welding mode. A soapstone was used to support the laminates. Induction welded panels, with a total welded length of 250 mm and an overlap width of 20 mm, were produced with this setup.

A K-type thermocouple with shielded cables, placed at the welding interface in contact with the two laminates and connected to a data logger, was able to measure the evolution of the interface temperature during welding. A laser pyrometer measured the surface temperature of the upper CF/LMPAEK laminate during welding.

3 | FINITE ELEMENT MODELING

Finite Element Analysis (FEA) of the electromagnetic field coupled with the heat transfer in solids was performed using COMSOL Multiphysics 4.4. The electromagnetic analysis was needed due to the alternating current in the coil and associated magnetic field, which induced eddy currents in nearby conductive materials. Eddy currents generated heat, and therefore a heat conduction problem was also studied. The model accounted for the coil motion at a constant speed and included a moving mesh approach.

Figure 3 reports the governing equations used in the model for the electromagnetic and temperature fields, that is, Maxwell's equations (1–4) coupled with a heat balance in solids (equation 5).[61] The heat source was given by the heat losses generated by eddy currents (equation 6), the heat released during matrix crystallization (equation 7) and the heat absorbed during matrix melting (equation 8). This latter term was subtracted from the generated heat since it refers to absorbed heat. Even if the contributions of the crystallization and melting of the matrix were quite small compared to the heat dissipated by the induced currents, these values were introduced in the FE model, as explained later, to predict the regions where matrix melting and crystallization occurred during welding.

The modeled geometry, reported in Figure 4, consisted of three distinct regions: an air domain around the

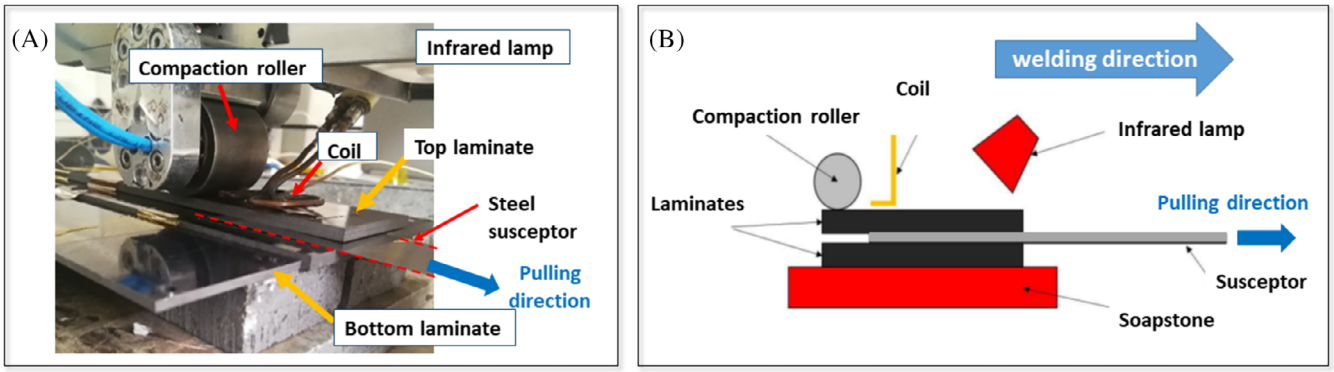

FIGURE 2 Continuous induction welding set-up with susceptor: (A) picture and (B) schematic representation.

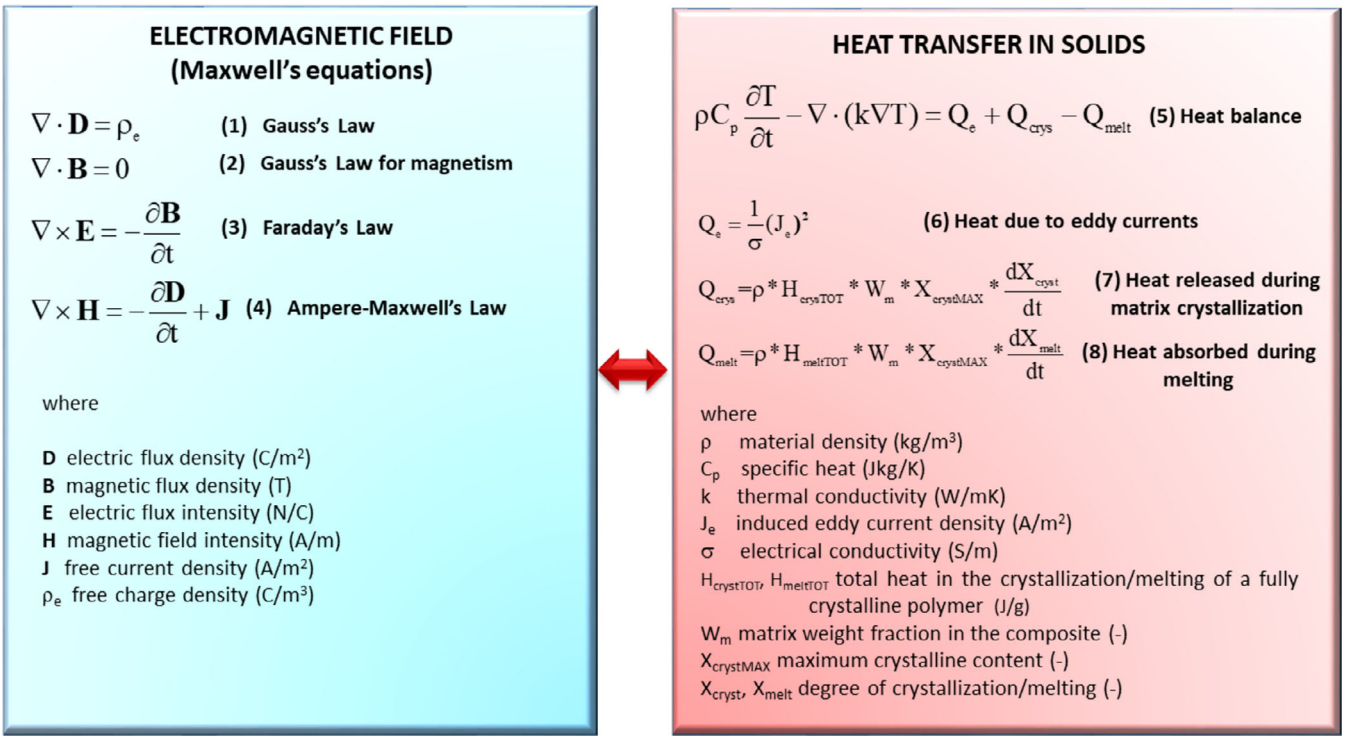

FIGURE 3 Governing equations of electromagnetic field and heat transfer in solids.

composite to simulate the propagation of electromagnetic fields and heat dissipation, the induction coil, and two partially overlapped composite plates with the susceptor. The susceptor in the model has not moved away as in the experiment to simplify the FEM model. Considering that the susceptor thickness was only 0.2 mm, that is, the thickness of a ply, the FE model included it as shown in Figure 5 (highlighted in yellow). However, a metal sheet between the two adherents, after they were in contact, could impact the heat exchange conditions due to its thermal conductivity being more than one order of magnitude higher than that of the composite laminates. To address this, the thermal properties of this central layer were altered from those of steel to those of the composite while the adherents were in contact, that is, in correspondence with the roller transit. Instead of a moving susceptor, "moving" material properties were implemented to overcome many numerical challenges in the FE model.

A 3D analysis was performed adopting a dense tetrahedral mesh (more than 10^5 nodes, determined after mesh optimization) for the solid volumes (i.e., composite and susceptor domains) while a coarser mesh was set for air domains. A mesh sensitivity study allowed us to evaluate the sensitivity of the solution to mesh density.

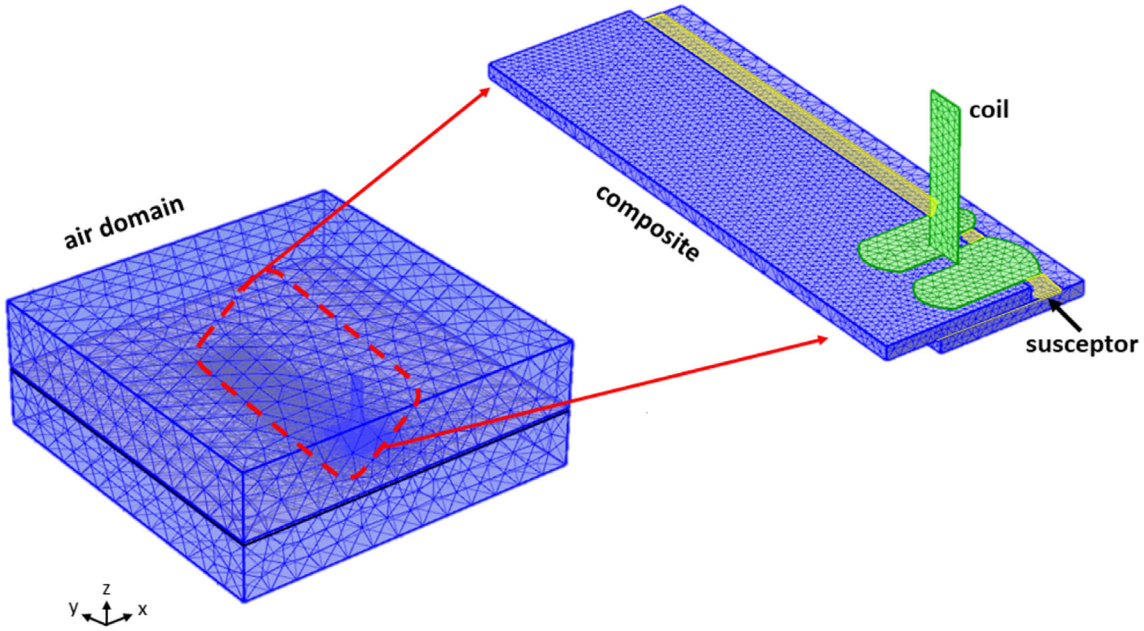

FIGURE 4 Modeled geometry. The susceptor and coil are highlighted in yellow and green, respectively.

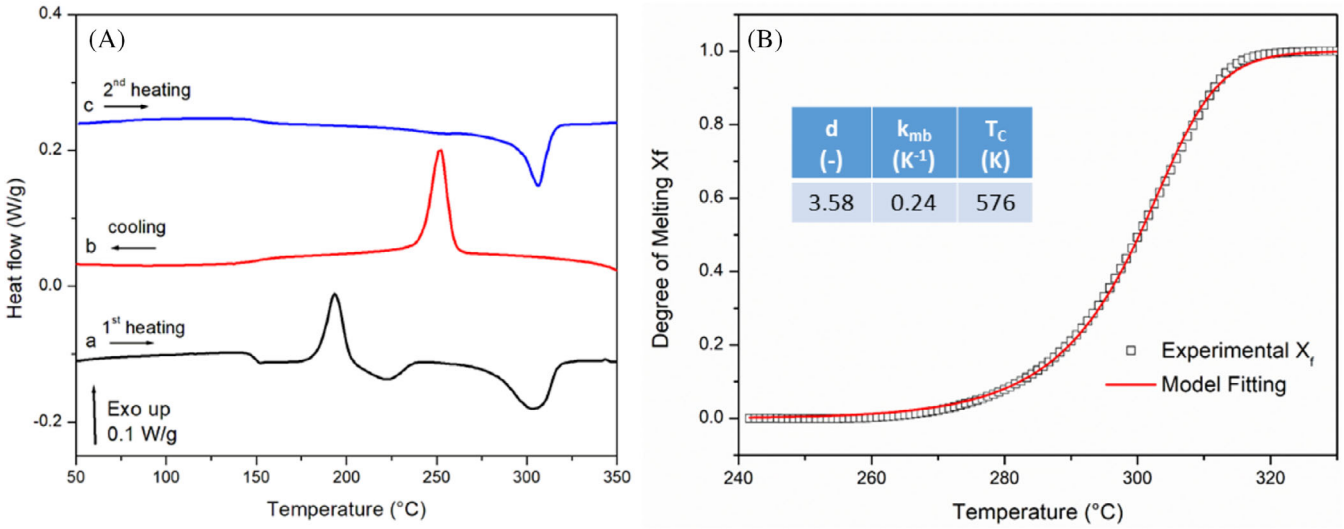

FIGURE 5 A) DSC thermogram of LMPAEK during first heating (A), cooling (B) and second heating (C) at 10 °C/min; (D) Model fitting of the degree of melting of LMPAEK as a function of temperature according to equation 2.

Thermal boundary conditions (BCs) were applied to the adherents, susceptor, and roller. A natural heat transfer coefficient of 5 W/(m^2 K) was adopted, except for the upper surfaces where the radiation from the IR lamp and the cooling of the contact roller were taken into account. To simplify the finite element model, the radiation from the infrared lamp and the cooling brought about by the roller were represented by equivalent convective heat transfer coefficients of 50 and 500 W/m^{2}K, respectively.

4 | RESULTS

4.1 | Kinetic study of the thermal behavior of LMPAEK matrix

The DSC thermograms of the LMPAEK matrix are reported in Figure 5A. During the first heating scan (curve a in Figure 5A), the glass transition temperature at 147 °C was followed by the cold crystallization and melting peak, centered at 193 and 305 °C, respectively. Upon cooling (curve b

in Figure 5A), the crystallization peak from the melt was found at 252 °C. The crystallization and melting behavior of the matrix played a crucial role in determining the appropriate processing parameters during induction welding. This allowed for accurate prediction of melting occurrence and whether crystallization took place during cooling as the compaction roller pressed the laminate.

Non-isothermal DSC data were employed for the melting and crystallization models incorporated in the FE model. The measured heat flow (dH/dt) was converted into the rate of melting, dX_m/dt, as described by Greco et al.[62]

$$\frac{dX_m}{dt} = \Delta H_m \left(\frac{dH}{dt}\right) \tag{1}$$

where X_m was the degree of melting, expressed by a value ranging from 0 to 1 and calculated by integration of Equation 1 across the melting peak as shown in Figure 5B. X_m (T) was assumed to be a cumulative distribution of the melting temperatures of lamellar crystal populations of different thicknesses. Therefore, a statistical-based approach was adopted to model X_m (T), as shown in Figure 5B:[62]

$$X_m(T) = 1 + (d-1)\exp\left[-k_{mb}(T - T_m)\right]^{\frac{1}{1-d}} \tag{2}$$

where $T_m = 576$ K was the melting peak temperature in Kelvin, and $d = 3.58$ and $k_{mb} = 0.24\ K^{-1}$ were the fitting parameters.

To model the crystallization degree X_c of LMPAEK during cooling from the melt at a variable cooling rate, the Jeziorny model was modified, accounting for the time dependence on the integral of the cooling rate.[63,64] X_c as a function of temperature was expressed as follows:

$$X_c(T) = 1 - \exp\left[-K(T)\cdot t^n\right] \tag{3}$$

where K(T) was a kinetic function of crystallization, t was the time, and n was the Avrami exponent. When the cooling was at a constant rate, β, the time was expressed as:

$$t = \frac{T - T_0}{\beta} \tag{4}$$

where T_0 was the initial temperature of the process. Replacing (4) into the Jeziorny equation (3):

$$X_c(T) = 1 - \exp\left[-K(T)\cdot\left(\frac{T - T_0}{\beta}\right)^n\right] \tag{5}$$

If K(T) followed an Arrhenius law:

$$K(T) = K_0 \exp\left(-\frac{E_a}{RT}\right) \tag{6}$$

where K_0 was a pre-exponential factor, E_a the activation energy, and R the gas constant. Substituting equation 6 into equation 5, an equation for calculating the degree of crystallization as a function of temperature during constant-rate cooling was obtained.

$$X_c(T) = 1 - \exp\left[-K_0 \exp\left(\frac{E_a}{RT}\right)\left(\frac{T_0 - T}{\beta}\right)^n\right] \tag{7}$$

Equation 7 for variable rate cooling became:

$$X_c(T) = 1 - \exp\left[-\int_{T_0}^{T} K_0 \exp\left(\frac{E_a}{RT}\right)\left(\frac{T_0 - T}{\beta(T)}\right)^n dT\right] \tag{8}$$

The curves of X_c versus temperatures, determined at different heating rates, were modeled for obtaining K_0, E_a, and n. The average values were reported in Figure 6B.

4.1.1 | Static induction heating experiments for the determination of electrical conductivity

Static induction heating tests were performed to determine the electrical conductivity of the composite laminate examined in this study. Electrical conductivity is known to be an anisotropic property that significantly depends on the fiber arrangement within each ply and the stacking sequence of the plies. These factors influence the number of closed loops between the fibers, where eddy currents can circulate. Given the lack of experimentally measured or literature data for the composite material in question, an iterative approach was employed, which is adaptable to different reinforcement types and lay-up. The proposed procedure lead to an indirect determination of the electrical conductivity σ by matching the measured and simulated temperature profiles during a static induction welding experiment. A previously developed and validated Finite Element (FE) model[65] for the static induction welding of CF reinforced polyphenylene sulfide was used for this purpose. The static induction heating tests were carried out using a low coil current (100 A) in order to have enough time to accurately measure the temperature.

Since the simulation required input values for σ_x, σ_y, and σ_z, the initial trial used electrical conductivity values obtained by Cortes et al.[66] on a similar material, that is, unidirectional CF/PEKK laminates with a fiber volume

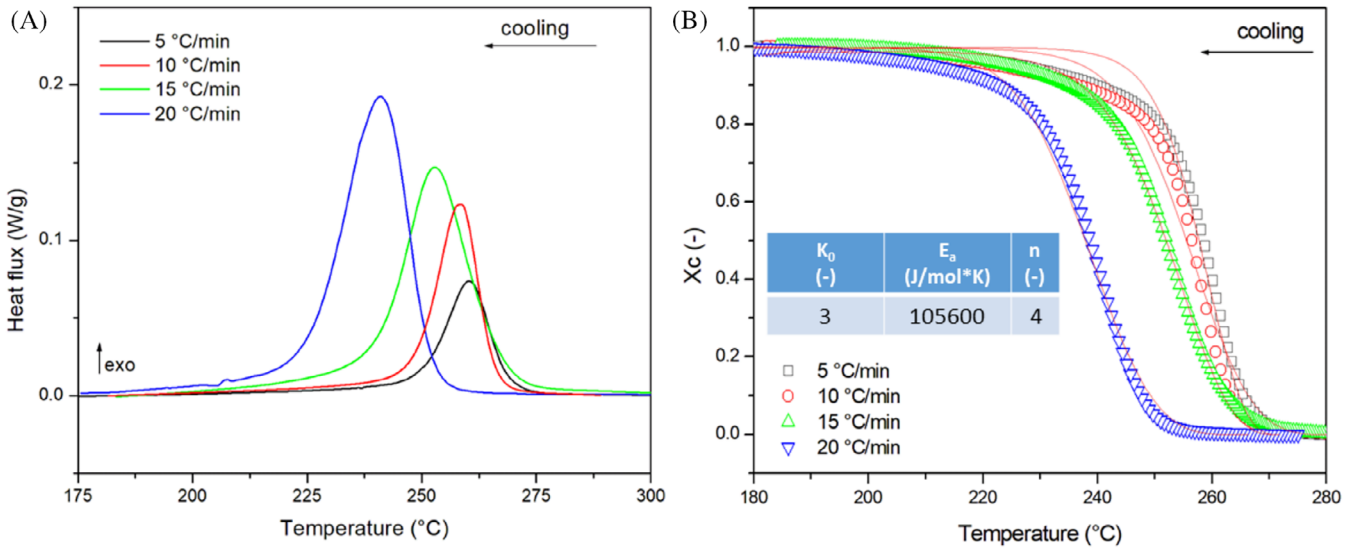

FIGURE 6 (A) DSC thermogram of CF/LMPAEK during cooling at different heating rates; (B) Model fitting of the degree of crystallization as a function of temperature.

fraction of 60%. These values were iteratively adjusted to achieve a close match between the experimental and simulated temperature profiles, as captured by a thermal camera (Figure 7). Upon completing this iterative process, the σ_x, σ_y, and σ_z values listed in Table 1 were identified as providing the best correspondence between the two thermal profiles. It is worth noting that the resulting temperature profile is similar to those obtained by Bensaid et al.[67] and Wasselynk et al.[68] for static induction welding of UD cross-ply laminates using low coil current.

4.2 | Numerical simulation of continuous induction welding

The FE model of continuous induction welding took into account the movement of the coil and the consolidation roller relative to the adherents. To this aim, the moving mesh approach of Comsol Multiphysics 4.4 was adopted, providing as input the displacement brought about by the coil speed.

Figure 8 shows temperature distribution maps at different times of CF/LMPAEK laminates during a continuous induction heating process with a coil moving at a speed of 2 mm/s. The inset provided the initial simulated geometry. As time progressed, the temperature maps revealed a clear rise, especially in the region directly exposed to the moving coil. The hottest region was located on the moving susceptor transferring heat to the two laminates. This created a localized heating zone with a temperature gradient. Heat spread outward, leaving the surrounding areas cool (around 100 °C, shown in blue), highlighting the localized heating and the slow heat transfer to adjacent regions. After the coil passed, the heated zone began to cool, with the cooling effect becoming more noticeable after contact with the compaction roller (indicated by the white-dotted rectangle).

At 16 s, a small region reached temperatures around 310 to 350 °C, while the rest of the laminate remained colder. The heat appeared concentrated in a narrow band under the coil. As time progressed, the heated region expanded and the peak temperature followed the coil movement, causing a gradual rise in the laminate surface temperature. Notably, the peak temperature directly under the coil remained constant, while the surface temperature of the top laminate was kept below 260 °C, a controlled parameter in the experimental setup to prevent surface melting during roller contact.

The simulated distribution of temperature and degree of melting at different times during continuous induction welding of a composite material with the coil moving at a speed of 2 mm/s is reported in Figure 9A,B. As the coil passed over the material, it induced localized heating in the composite, causing the thermoplastic matrix to melt, as reflected in both the temperature and degree of melting distributions. At each time step, the interface region under the coil reached temperatures between 310 and 400 °C (red-orange region), which was sufficient to melt the thermoplastic matrix, avoiding any degradation. The temperature gradient indicated a slow heat dissipation from the weld zone to the surrounding areas, with most of the material remaining relatively cool (blue, below 150 °C) compared to the narrow region where adherents were in contact directly under the coil. As time progressed, the high-temperature region extended along the laminate in

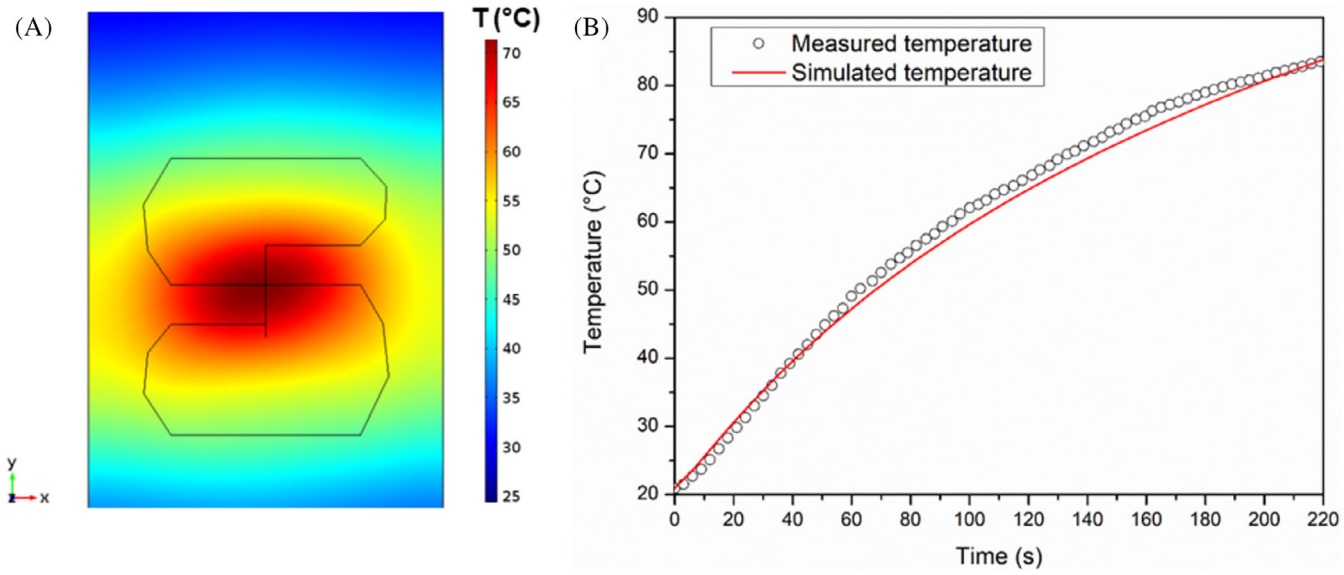

FIGURE 7 Static induction heating of CF/LMPAEK laminates: (A) simulated temperature field at the surface, (B) comparison between the measured and simulated temperature profile at the top surface.

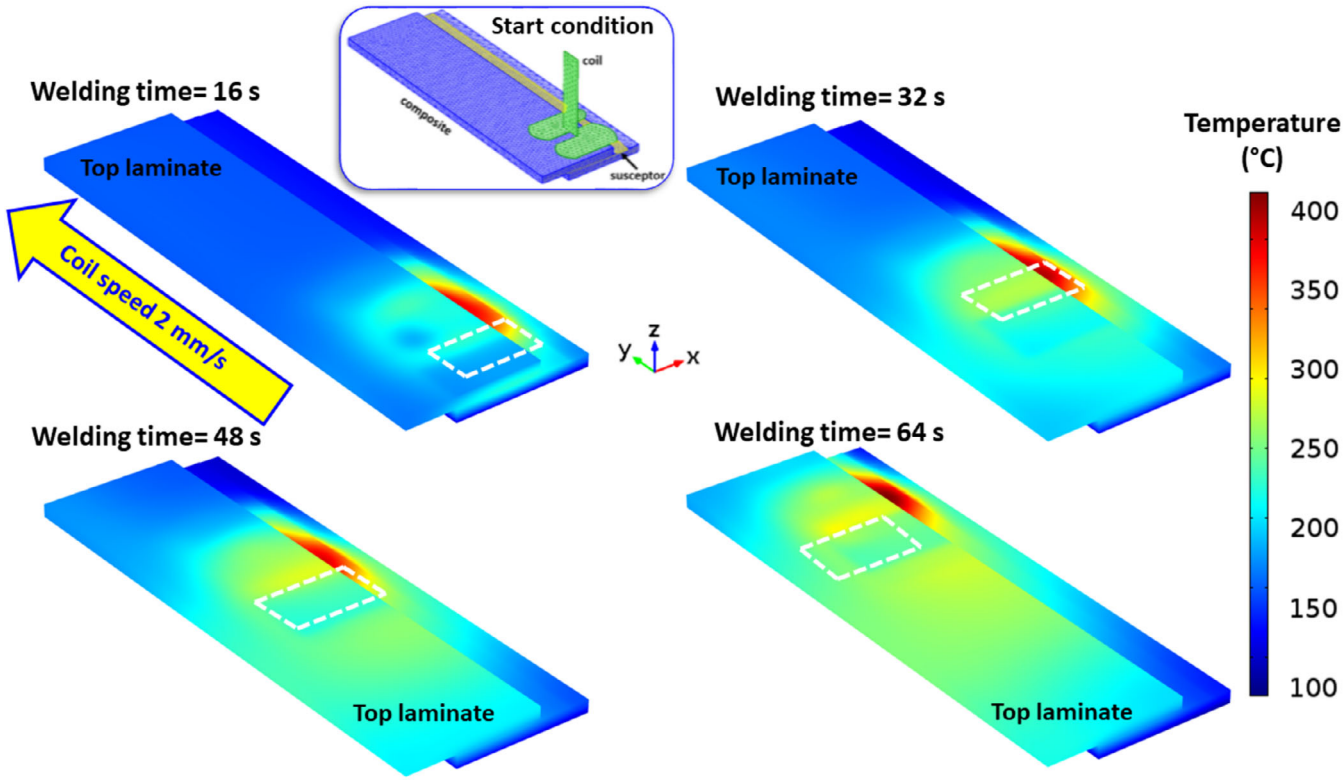

FIGURE 8 Continuous induction heating of CF/LMPAEK laminates: Temperature maps at different times for a coil speed of 2 mm/s. In the inset, the geometry at the initial condition (time = 0 s) is reported.

the direction of the coil movement; consequently, the molten zone increased in size and more material exhibited partial or complete melting. The temperature distribution in the thickness direction at 16 s is reported in Figure 9C. The results in Figure 9 demonstrated how only the interface reached melting thanks to the boundary conditions, which limited the surface temperature. The FE model of continuous induction welding of CF/LMPAEK laminates

with a movable susceptor was validated by comparing simulation results to experimental data obtained by a thermocouple at the welding interface, as shown in Figure 9D. The simulation and experimental data matched very closely, especially during the initial temperature rise, showing a sharp increase that peaked around 34 s. A heating rate of 10.6 °C/s was measured and predicted, resulting comparable with that one obtained by Farahani et al.[36] on carbon fiber-reinforced polyphenylene sulphide (PPS) using a susceptor consisting in a PPS film made conductive by dispersed silver nanoparticles.

The difference in the peak temperature between the measured and predicted data plots was very small (less than 2%). After the peak, both the experimental and simulation data evidenced a decrease in temperature with a shoulder related to the passage of the roller. In this region, the simulation (red line) started to deviate from the experimental data. The latter displayed a more gradual cooling.

The different temperature evolution during cooling could result from differences between the simulation geometry and the actual one. In the experimental set-up, a full contact between the laminates occurred after the susceptor was removed, allowing the roller pressure to weld the molten matrix at the laminate surface. At this stage, cooling was slightly better predicted by FE, which assumed full contact between the welding surfaces. However, the actual cooling rate was lower than the simulated one, likely due to the gap in the baseplate of soapstone and a possible thin air gap inside the hole where the thermocouple was housed, which acted as an insulator.

With the industry's shift toward faster production for improved efficiency, shorter cycle times, and reduced power consumption per unit, simulations have been conducted with increased coil speed. As an example, Figure 10A reports the 3D surface plot showing the changes in temperature as a function of current intensity and time during continuous induction welding of UD composites at a constant speed of 5 mm/s. All the plots demonstrate a rapid temperature rise within about 12 s, with a higher peak temperature at a higher current intensity. The optimization of coil current to produce the desired induction heating at the required speed is mandatory and can be easily obtained with the simulation, avoiding the time-and cost-consuming experimental trials.

As demonstrated by Wang et al.,[69] optimal heat input is crucial for fusion behavior at the bonding interface.

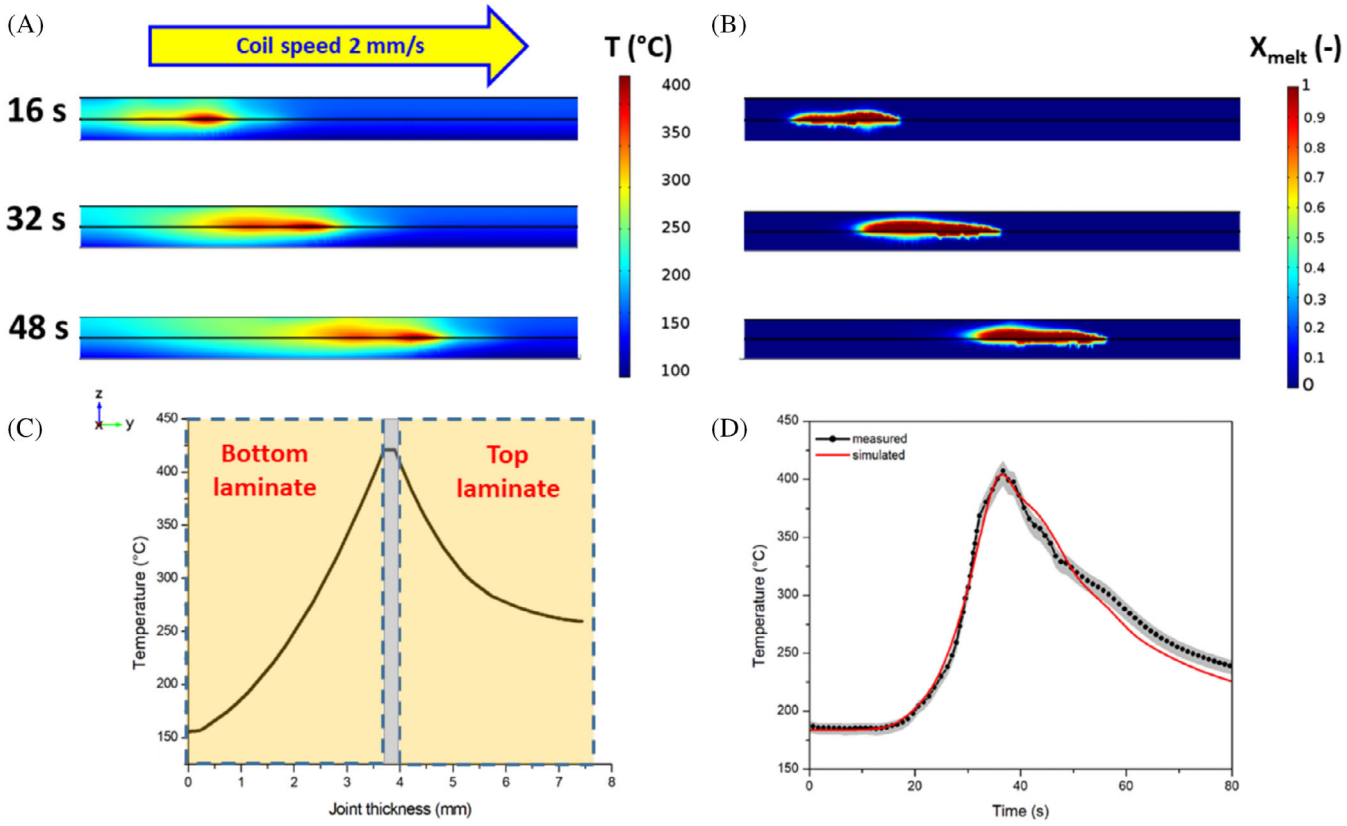

FIGURE 9 Simulation results during continuous induction welding at a coil speed of 2 mm/s: (A) temperature and (B) degree of melting distribution at different times; (C) temperature distribution in thickness direction at 16 s; (D) comparison between measured and simulated temperature profile at the welding interface during the susceptor-aided induction welding. The area in gray represents the standard deviation of the experimental data.

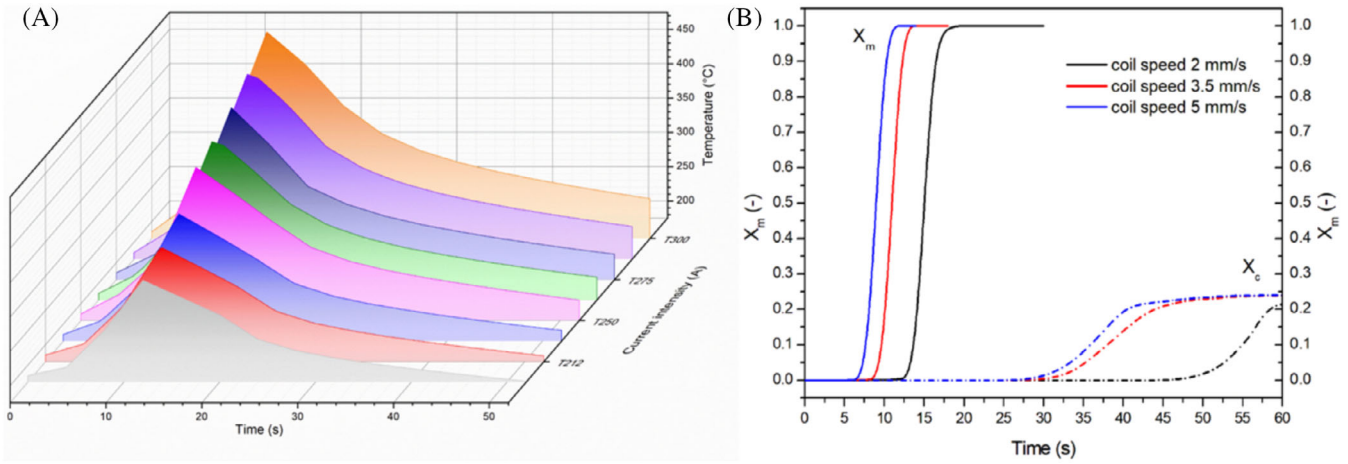

FIGURE 10 (A) 3D surface plot showing the changes of temperature as a function of current intensity (A) and time (s) during continuous induction welding of UD composites at a constant speed of 5 mm/s; (B) temporal evolution of the degree of melting (X_m) and degree of crystallization (X_c) at different coil speeds.

Insufficient heat results in unfused gaps, while excessive heat leads to overheating and resin decomposition. Faster welding speeds may result in incomplete melting of the matrix, which can compromise the quality of the weld. Therefore, it is very important to simulate the melting and crystallization behavior at various coil speeds to optimize the welding parameters effectively. In Figure 10B, the temporal evolution of the degree of melting (X_m) and degree of crystallization (X_c) is reported for different coil speeds. As coil speed increased, the onset of melting occurred later, and the transition to full melting happened more rapidly. This implied that the heating rate was highly dependent on the coil speed. At higher coil speeds (e.g., 5 mm/s), the time at which the system reached the maximum temperature was shorter, leading to less time for complete melting. This behavior contrasted with lower coil speeds (e.g., 2 mm/s), where the longer time at high temperature allowed for more complete melting. The crystallization degree showed a notable decrease with increasing speed, reflecting the limited time for crystallization during the cooling phase at higher speeds. This could significantly impact the mechanical properties of the welded material. The observed trends suggest that an intermediate coil speed might balance melting efficiency and crystallinity retention, ensuring both productivity and quality. While higher speeds may enhance production efficiency, they can adversely affect the thermal history of the weld zone, potentially leading to incomplete melting and lower crystallinity.

4.3 | Evaluation of the weld quality

Figure 11 shows a representative cross-sectional micrograph of the induction-welded CF/LMPAEK joint. The image reveals a seamless interface between the layers, indicating effective melting of the adherent matrix and strong adhesion between the CF/LMPAEK layers and the intermediate glass fiber layer.

The weld quality of the induction welded CF/LMPAEK joints was evaluated by measuring shear strength in single-lap shear tests and analyzing failure modes. The shear strength was calculated by dividing the maximum load by the overlap area of the weld. An average value of 25.55 ± 0.8 MPa was obtained. This value was in agreement with literature data for induction welded joints made of unidirectional CF/PEEK (24.7 ± 0.5 MPa[37]) or unidirectional CF/PEKK with a conductive susceptor made of PEKK nanofilled with 60 wt% Ag nanoparticles (20.9 ± 1.1 MPa[39]).

The fracture surfaces reported in Figure 12A suggested a predominant interlaminar failure mode with failure occurring within the composite material rather than at the weld interface. This suggests that the induction welded joint was stronger than the surrounding material. Scanning electron microscopy (SEM) and atomic force microscopy (AFM) were used to analyze the fracture surfaces of the welded joints tested in lap shear. As shown in Figure 12B–D, some areas of the fracture surfaces exhibited resin accumulation with minimal fiber breakage. In most regions, fibers were coated by matrix. AFM images further confirmed the presence of resin-rich regions (Figure 12E,F) and matrix-coated fibers (Figure 12G). These analyses revealed separated plies with relatively rough surfaces, indicating the prevalence of an interlaminar failure in the welded joints with very little fiber fracture. These results confirmed the good consolidation of the joint as failure occurred primarily between the composite plies rather than at the weld interface.

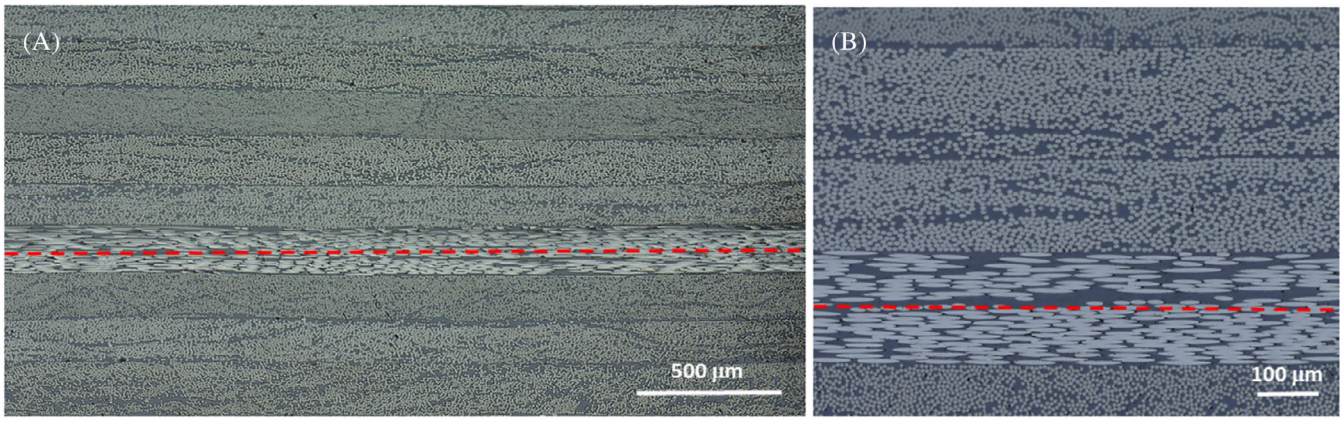

FIGURE 11 Cross-section optical micrograph of induction welded CF/LMPAEK joint. The welding line is evidenced by the red dotted line.

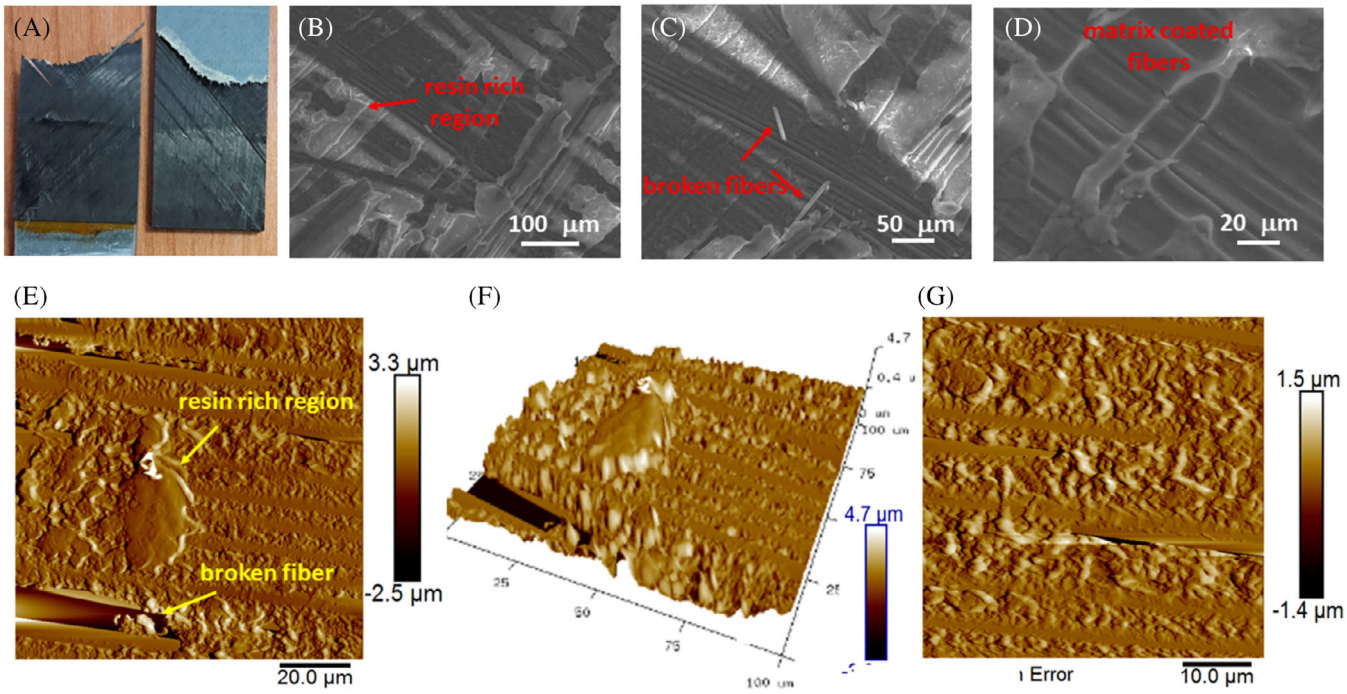

FIGURE 12 (A) fracture surfaces of welded joints; (B–D) SEM micrographs of the fracture surfaces; (E,F) AFM images of the fracture surfaces.

The evaluation of the weld quality indicated the achievement of a reliable and high-quality weld in the composite material. However, the long-term reliability of the joints is also an important aspect for industrial applications of each welded joint, independent of the used welding technology. Previous studies have demonstrated that thermal aging of CF/PEEK at moderate temperatures (250 °C) can improve crystallinity and crystal perfection of the thermoplastic matrix, while at higher temperatures (300 °C), after an initial increase, crystallinity significantly decreases due to degradation and cross-linking.[70] Therefore, it is expected that prolonged exposure to high temperatures and oxidative environments can lead to matrix degradation, changes in crystallinity, and reduced mechanical properties over time in thermoplastic composite welds.[71] However, since investigations on the durability of induction-welded CF/LMPAEK joints under service conditions require extensive long-term testing protocols, they are beyond the scope of this work but are the subject of a future study. Finally, the proposed method has been applied to additional carbon fiber reinforced laminates with different stacking sequences. These analyses confirmed the method's effectiveness across different composite architectures.

5 | CONCLUSIONS

This study demonstrated the feasibility of using a removable steel susceptor to assist the continuous induction welding of unidirectional carbon fiber laminates with a low melting Polyaryletherketone matrix. The susceptor was connected to the welding head and moved at the same speed as the induction coil along the weld line, but it did not remain at the welding interface, thus preventing the properties reduction of the welded joint.

A 3D electromagnetic Finite Element (FE) model coupled to a 3D thermal FE model was developed to evaluate the induction heating of UD laminates during continuous induction welding. The electrical conductivity of the analyzed composite was determined with an iterative procedure based on an FE model of static induction welding. The temperature distribution on the susceptor and at the interface between the two laminates was accurately predicted and validated by temperature measurements.

The model was validated by comparing the simulation results with experimentally obtained time versus temperature curves. As the coil passed over the material, it induced localized heating in the composite, causing the thermoplastic matrix to melt, as reflected in both the temperature and melting degree distributions. The results showed that the melting process was highly localized, necessitating precise control to prevent incomplete bonding or overheating. The degree of melting was highly concentrated directly under the coil.

The findings of this study have broader implications, as this methodology could be adapted to other materials or processes requiring precise thermal control. The integration of simulation, experimental validation, and practical implementation offers a model for addressing other advanced manufacturing challenges.

AUTHOR CONTRIBUTIONS

Francesca Lionetto: Validation, Investigation, Supervision, Formal analysis, Writing – review & editing, Writing – original draft. **Giulio Zecca**: Methodology, Investigation. **Giuseppe Buccoliero**: Methodology, Investigation. **Sonia Bagheri**: Investigation. **Claudio Mele**: Investigation, Writing – review & editing.

ACKNOWLEDGMENTS

The authors would like to express their sincere gratitude to Professor Alfonso Maffezzoli for his invaluable guidance, support, and mentorship throughout the course of this work. Dr. Antonio Notarangelo and Mr. Michele Arganese (Cetma, Italy) are kindly acknowledged for their support in the induction welding of composite laminates. Mr. Donato Cannoletta (University of Salento) and Dr. Federica De Riccardis (ENEA) are kindly acknowledged for their support in SEM and optical microscopy. Open access publishing facilitated by Universita del Salento, as part of the Wiley - CRUI-CARE agreement.

DATA AVAILABILITY STATEMENT

The data that support the findings of this study are available from the corresponding author upon reasonable request.

ORCID

Francesca Lionetto https://orcid.org/0000-0003-4466-1161

REFERENCES

1. Marinis D, Markatos D, Farsari E, Amanatides E, Mataras D, Pantelakis S. A novel plasma-enhanced solvolysis as alternative for recycling composites. *Polym Basel*. 2024;16:2836.
2. Pegoretti A. Towards sustainable structural composites: a review on the recycling of continuous-fiber-reinforced thermoplastics. *Adv Ind Eng Polym Res*. 2021;4:105-115.
3. Iqbal Z, Siddique A, Nawab Y, Shaker K. A comparative static and dynamic behavior of thermoplastic composite joints produced using different joining techniques. *Polym Compos*. 2023;44:4853-4861.
4. Lionetto F, Moscatello A, Totaro G, Raffone M, Maffezzoli A. Experimental and numerical study of vacuum resin infusion of stiffened carbon fiber reinforced panels. *Mater Basel*. 2020;13(21):4800. doi:10.3390/ma13214800
5. Filippatos A, Markatos D, Tzortzinis G, et al. Sustainability-driven Design of Aircraft Composite Components. *Aerospace*. 2024;11(86):1-20.
6. Yamamoto T, Nakamoto T, Irisawa T. Carbon fiber-reinforced thermoplastic synthesized by the Hypercrosslinking reaction of polyether ether ketone. *Polym Compos*. 2024;45:11473-11479.
7. Hidalgo-Salazar MA, Correa-Aguirre JP, Román AJ, Gonzalez R, Vera R, Osswald TA. Colombian natural fibers: potential applications in sustainable natural fiber reinforced composites materials. *Polym Compos*. 2024. doi:10.1002/pc.29313
8. Lionetto F, Montagna F, Natali D, et al. Correlation between elastic properties and morphology in short fiber composites by X-Ray computed micro-tomography. *Compos Part A Appl Sci Manuf*. 2021;140:106169.
9. De Pascalis F, Lionetto F, Maffezzoli A, Nacucchi M. A general approach to calculate the stiffness tensor of short-fiber composites using the fabric tensor determined by X-ray computed tomography. *Polym Compos*. 2023;44:917-931.
10. ten Bruggencate I, van Hattum FWJ, Meuzelaar J, de Bruijn T. Recycled carbon fiber reinforced polyphenylene sulphide in aerospace. *Proceed Int SAMPE Tech Conf*. 2024. doi:10.33599/nasampe/s.24.0097
11. Lionetto F, Corcione CE, Rizzo A, Maffezzoli A. Production and characterization of polyethylene terephthalate nanoparticles. *Polym Basel*. 2021;13:3745. doi:10.3390/polym13213745
12. Lionetto F, Esposito Corcione C, Messa F, Perrone S, Salomone A, Maffezzoli A. The sorption of amoxicillin on engineered polyethylene terephthalate microplastics. *J Polym Environ*. 2023;31:1383-1397.

13. Huang Y, Gao X, Zhang Y, Ma B. Laser joining Technology of Polymer-Metal Hybrid Structures-a Review. *J Manuf Process*. 2022;79:934-961.
14. Scarselli G, Castorini E, Panella FW, Nobile R, Maffezzoli A. Structural behaviour modelling of bolted joints in composite laminates subjected to cyclic loading. *Aerosp Sci Technol*. 2015;43:89-95.
15. Lambiase F, Yanala PB, Leone C, Paoletti A. Repairing aluminum-PEEK hybrid metal-polymer joints made by thermo-mechanical joining. *J Manuf Process*. 2023;93:1-14. doi: 10.1016/j.jmapro.2023.03.018
16. Cheng Y, Yu R, Zhou Q, Chen H, Yuan W, Zhang Y. Real-time sensing of gas metal arc welding process–a literature review and analysis. *J Manuf Process*. 2021;70:452-469.
17. Mehdikhani H, Mostafapour A, Laieghi H, Najjar R, Lionetto F. Mechanical and microstructural properties of HDPE pipes manufactured via orbital friction stir welding. *Mater Basel*. 2022;15:3810. doi:10.3390/ma15113810
18. Jin T, Ma Y, Xiong Z, et al. Bioinspired, tree-root-like interfacial designs for structural batteries with enhanced mechanical properties. *Adv Energy Mater*. 2021;11:1-8. doi:10.1002/aenm.202100997
19. Liu S, Wang Y, Fan T, Wu Z, Li Y. The influence of process parameters and carbon nanotubes on composite material joints. *Polym Compos*. 2024;45:14875-14887.
20. Brito CBG, Teuwen J, Dransfeld CA, Villegas IF. On improving process efficiency and weld quality in ultrasonic welding of misaligned thermoplastic composite adherends. *Compos Struct*. 2023;304:116342.
21. Khatri B, Roth MF, Balle F. Ultrasonic welding of additively manufactured PEEK and carbon-fiber-reinforced PEEK with integrated energy directors. *J Manuf Mater Process*. 2022;7(2): 1-12.
22. Liu Z, Li Y, Liu Z, Yang Y, Li Y, Luo Z. Ultrasonic welding of metal to fiber-reinforced thermoplastic composites: a review. *J Manuf Process*. 2023;85:702-712.
23. Reis JP, de Moura M, Samborski S. Thermoplastic composites and their promising applications in joining and repair composites structures: a review. *Mater Basel*. 2020;13:5832.
24. Banik N. A review on the use of thermoplastic composites and their effects in induction welding method. *Mater Today Proc*. 2018;5:20239-20249.
25. Nicassio F, Maffezzoli A, Buccoliero G, Scarselli G. Shear buckling of aerospace panels made by induction welded thermoplastic matrix composite elements. *Polym Compos*. 2022;43: 4544-4555.
26. Lambiase F, Scipioni SI, Lee C-J, Ko D-C, Liu F. A state-of-the-art review on advanced joining processes for metal-composite and metal-polymer hybrid structures. *Mater Basel*. 2021;14: 1890.
27. Li X, Bu H, Wang F, Li B, Yao J, Zhan X. Numerical simulation and experimental verification of temperature field in induction welding process of CFRTP L-shaped stringer and skin based on magneto-thermal coupling. *Int J Adv Manuf Technol*. 2024;130: 4341-4357.
28. Villegas IF, Moser L, Yousefpour A, Mitschang P, Bersee HE. Process and performance evaluation of ultrasonic, induction and resistance welding of advanced thermoplastic composites. *J Thermoplast Compos Mater*. 2013;26:1007-1024.
29. Modi V, Bandaru AK, Ramaswamy K, et al. Repair of impacted thermoplastic composite laminates using induction welding. *Polym Basel*. 2023;15:3238.
30. Bayazeid SM, Poon K-L, Subeshan B, Alamir M, Asmatulu E. Recovery of impact-damaged carbon fiber–reinforced composites using induction heating. *J Compos Mater*. 2022;56:605-618.
31. Varma M, Chandran S, Vijay Kumar V, Suyambulingam I, Siengchin S. A comprehensive review on the machining and joining characteristics of natural fiber-reinforced polymeric composites. *Polym Compos*. 2024;45:4850-4875.
32. Mariani A, Malucelli G. Insights into induction heating processes for polymeric materials: an overview of the mechanisms and current applications. *Energies*. 2023;16:4535.
33. Lionetto F, Pappadà S, Buccoliero G, Maffezzoli A. Finite element modeling of continuous induction welding of thermoplastic matrix composites. *Mater Des*. 2017;120:212-221.
34. Grouve WJB, Sacchetti F, Vruggink EJ, Akkerman R. Simulating the induction heating of cross-ply C/PEKK laminates–sensitivity and effect of material variability. *Adv Compos Mater*. 2021;30:409-430.
35. Khurshid MF, Hasan MMB, Abdkader A, Cherif C. Processing of waste carbon and polyamide fibers for high performance thermoplastic composites: a novel manufacturing Technology for Unidirectional Tapes Structure. *J Ind Text*. 2022;51:7256S-7276S.
36. Farahani RD, Janier M, Dubé M. Conductive films of silver nanoparticles as novel susceptors for induction welding of thermoplastic composites. *Nanotechnology*. 2018;29:125701.
37. Choi B-K, Kang C-S, Yoo M-H, Seo M-K. Effect of processing parameters on bonding performance of a carbon fiber/Polyetheretherketone thermoplastic composite prepared by induction welding. *Mater Basel*. 2023;16:3954.
38. Yarlagadda S, Kim HJ, Gillespie JW, Shevchenko NB, Fink BK. A study on the induction heating of conductive fiber reinforced composites. *J Compos Mater*. 2002;36:401-421.
39. Hoang V-T, Lee D-S, Kweon J-H, Kwak B-S, Nam Y-W. Multifunctional heating film as susceptor for induction-welded single-lap carbon fiber reinforced Polyetherketoneketone thermoplastic composite joints: thermal and mechanical behavior. *J Reinf Plast Compos*. 2023;43(17-18):07316844231198309. doi: 10.1177/07316844231198309
40. Dei Sommi A, Buccoliero G, Lionetto F, De Pascalis F, Nacucchi M, Maffezzoli A. A finite element model for the prediction of porosity in autoclave cured composites. *Compos B Eng*. 2023;264:110882.
41. Ahmed TJ, Stavrov D, Bersee HEN, Beukers A. Induction welding of thermoplastic composites—an overview. *Compos Part A Appl Sci Manuf*. 2006;37:1638-1651.
42. Yu H, Heider D, Advani S. A 3D microstructure based resistor network model for the electrical resistivity of unidirectional carbon composites. *Compos Struct*. 2015;134:740-749. doi:10.1016/j.compstruct.2015.08.131
43. O'Shaughnessey PG, Dubé M, Villegas IF. Modeling and experimental investigation of induction welding of thermoplastic composites and comparison with other welding processes. *J Compos Mater*. 2016;50:2895-2910.
44. de Wit AJ, van Hoorn N, Straathof LS, Vankan WJ. Numerical simulation of inductive heating in thermoplastic unidirectional cross-ply laminates. *Front Mater*. 2023;10:1155322.
45. Polydoropoulou P, Cosma L, Labeas G, Markatos D, Dotoli R, Felline F. Simulating the induction welding process of thermoplastic composite materials for aircraft structures. *Aircraft Eng Aerosp Technol*. 2024;97(1):120-127. doi:10.1108/AEAT-04-2024-0116

46. Zhao Q, Zhang K, Zhu S, et al. Review on the electrical resistance/conductivity of carbon fiber reinforced polymer. *Appl Sci*. 2019;9:2390.
47. Li M, Wen L, Wang S, Liang J, Hou X. Multifactor optimization for induction welding of carbon fiber reinforced thermoplastic composites based on response surface methodology. *Polym Compos*. 2024;45(5):4307-4318. doi:10.1002/pc.28060
48. Yan X, Qiao L, Tan H, et al. Effect of carbon nanotubes on the mechanical, crystallization, electrical and thermal conductivity properties of CNT/CCF/PEKK composites. *Mater Basel*. 2022;15:4950.
49. Pérez-Martín H, Mackenzie P, Baidak A, Brádaigh CMÓ, Ray D. Crystallisation behaviour and morphological studies of PEKK and carbon fibre/PEKK composites. *Compos Part A Appl Sci Manuf*. 2022;159:106992.
50. Pérez-Martín H, Buchalik-Bopp S, Guettler BE, et al. Effect of crystallinity and morphology on the mechanical properties of CF/PEKK composites manufactured under compression Moulding and automated tape placement. *Mater Today Commun*. 2023;36:106442.
51. Marinosci V, Chen K, Helthuis NGJ, et al. Direct observation of the fracture behavior of the polyether ketone ketone (PEKK) spherulites. *J Appl Polym Sci*. 2024;141:1-11. doi:10.1002/app.54764
52. Tao W, Su X, Wang H, Zhang Z, Li H, Chen J. Influence mechanism of welding time and energy director to the thermoplastic composite joints by ultrasonic welding. *J Manuf Process*. 2019;37:196-202.
53. Wilkins LT, Strauss AM. Post-weld annealing of friction stir welded carbon fiber reinforced low-melt Polyaryletherketone. *J Compos Mater*. 2023;57:4589-4601.
54. Audoit J, Rivière L, Dandurand J, Lonjon A, Dantras E, Lacabanne C. Thermal, mechanical and dielectric behaviour of poly (aryl ether ketone) with low melting temperature. *J Therm Anal Calorim*. 2019;135:2147-2157.
55. Yi N, Davies R, Chaplin A, McCutchion P, Ghita O. Slow and fast Crystallising poly aryl ether ketones (PAEKs) in 3D printing: crystallisation kinetics, morphology, and mechanical properties. *Addit Manuf*. 2021;39:101843.
56. Martín I, Fernández K, Cuenca J, Sánchez C, Anaya S, Élices R. Design and manufacture of a reinforced fuselage structure through automatic laying-up and in-situ consolidation with Co-consolidation of skin and stringers using thermoplastic composite materials. *Heliyon*. 2023;9(1):e12728. doi:10.1016/j.heliyon.2022.e12728
57. Schiel I, Raps L, Chadwick AR, Schmidt I, Simone M, Nowotny S. An investigation of in-situ AFP process parameters using CF/LM-PAEK. *Adv Manuf Polym Compos Sci*. 2020;6:191-197.
58. Lionetto F, Dell'Anna R, Montagna F, Maffezzoli A. Modeling of continuous ultrasonic impregnation and consolidation of thermoplastic matrix composites. *Compos Part A Appl Sci Manuf*. 2016;82:119-129.
59. TORAY CARBON FIBERS AMERICA T700G Technical Datasheet.
60. Audoit J, Cortes LQ, Racagel S, Lonjon A, Dantras E, Lacabanne C. Conductive sizing for improving electrical conductivity of carbon fiber/Polyaryl ether ketone/AgNWs composites. *J Appl Polym Sci*. 2019;136:47872.
61. Kang C, Shi C, Liu Z, et al. Research on the optimization of welding parameters in high-frequency induction welding pipeline. *J Manuf Process*. 2020;59:772-790.
62. Greco A, Maffezzoli A. Polymer melting and polymer powder sintering by thermal analysis. *J Therm Anal Calorim*. 2003;72:1167-1174.
63. Jeziorny A. Parameters characterizing the kinetics of the non-isothermal crystallization of poly (ethylene terephthalate) determined by DSC. *Polymer*. 1978;19:1142-1144.
64. Qiu Z, Yang W. Isothermal and nonisothermal melt crystallization kinetics of a novel poly (aryl ether ketone ether ketone ketone) containing a meta-phenyl linkage. *J Appl Polym Sci*. 2006;102:4775-4779.
65. Pappadà S, Salomi A, Montanaro J, Passaro A, Caruso A, Maffezzoli A. Fabrication of a thermoplastic matrix composite stiffened panel by induction welding. *Aerosp Sci Technol*. 2015;43:314-320.
66. Cortes LQ, Racagel S, Lonjon A, Dantras E, Lacabanne C. Electrically conductive carbon fiber/PEKK/silver nanowires multifunctional composites. *Compos Sci Technol*. 2016;137:159-166.
67. Bensaid S, Trichet D, Fouladgar J. Electromagnetic and thermal behaviors of multilayer anisotropic composite materials. *IEEE Trans Magn*. 2006;42:995-998.
68. Wasselynck G, Trichet D, Ramdane B, Fouladgar J. Microscopic and macroscopic electromagnetic and thermal modeling of carbon fiber reinforced polymer composites. *IEEE Trans Magn*. 2011;47:1114-1117.
69. Wang F, Zhang P, Luo J, Li B, Liu G, Zhan X. Effect of heat input on temperature characteristics and fusion behavior at bonding Interface of CFRTP induction welded joint with carbon fiber susceptor. *Polym Compos*. 2023;44:1586-1602.
70. Ma X, Wen L, Wang S, Lei M, Hou X. Effect and mechanism of thermal aging on mechanical properties of continuous carbon fiber-reinforced PEEK composite laminates. *Polym Compos*. 2024;45:13256-13271.
71. Mazur RL, Cândido GM, Rezende MC, Botelho EC. Accelerated aging effects on carbon fiber PEKK composites manufactured by hot compression molding. *J Thermoplast Compos Mater*. 2016;29:1429-1442.

SUPPORTING INFORMATION

Additional supporting information can be found online in the Supporting Information section at the end of this article.

How to cite this article: Lionetto F, Zecca G, Buccoliero G, Bagheri S, Mele C. Experimental and numerical investigation of susceptor-aided continuous induction welding of low-melt PAEK composites. *Polym Compos*. 2025;1-16. doi:10.1002/pc.29732